Ref. SISSA 13/99/EP
February 1999
hep-ph/9903303

Enhancing the Seasonal Variation Effect in the Case of the Vacuum Oscillation Solution of the Solar Neutrino Problem

M. Maris[a] and S.T. Petcov [b,c)*]

a) Osservatorio Astronomico di Trieste, I-34113 Trieste, Italy

b) Scuola Internazionale Superiore di Studi Avanzati, I-34013 Trieste, Italy

c) Istituto Nazionale di Fizica Nucleare, Sezione di Trieste, I-34013 Trieste, Italy

Abstract

We study in detail the threshold energy dependence of the seasonal variation effect in the energy integrated solar neutrino signal of the Super-Kamiokande detector in the case of the $\nu_e \leftrightarrow \nu_{\mu,\tau}$ vacuum oscillation (VO) solution of the solar neutrino problem. We show, in particular, that for the values of Δm^2 and $\sin^2 2\theta$ from the VO solution region, the predicted time and threshold e^- energy ($T_{e,Th}$) dependence of the event rate factorize to a high degree of accuracy. As a consequence, the VO generated seasonal variation asymmetry is given by the product of an time-independent function of $T_{e,Th}$ and the standard geometrical asymmetry. For any given Δm^2 and $\sin^2 2\theta$ from the VO solution region there exists at least one value of $T_{e,Th}$ from the interval $(5 - 11)$ MeV, for which the seasonal variation effect in the solar neutrino sample of events, formed by recoil electrons with kinetic energy $T_e \geq T_{e,Th}$, is either maximal or very close to the maximal; it can vary dramatically with $T_{e,Th}$. One can effectively search for the VO induced seasonal effect by forming a set of samples of solar neutrino events, corresponding to a sufficiently large number of different values of $T_{e,Th}$ from the indicated interval and by measuring the seasonal variation in each of these samples. Predictions for the magnitude of the seasonal effect in such samples are given for a large set of representative values of Δm^2 and $\sin^2 2\theta$ from the VO solution region.

---

*Also at: Institute of Nuclear Research and Nuclear Energy, Bulgarian Academy of Sciences, BG–1784 Sofia, Bulgaria.

1. Introduction

The hypothesis that the solar neutrinos undergo vacuum oscillations into muon and/or tau neutrinos, $\nu_e \leftrightarrow \nu_{\mu,\tau}$, when they travel from the Sun to the Earth [1–7] continues to be a viable and very appealing explanation [8,9] of the observed deficit of solar neutrinos [1] [10–15]. The mean event rate data from the solar neutrino experiments Homestake, Kamiokande, SAGE, GALLEX and Super-Kamiokande, can be described in terms of two-neutrino $\nu_e \leftrightarrow \nu_{\mu(\tau)}$ oscillations if the values of the two parameters, Δm^2 and $\sin^2 2\theta$, characterizing the oscillations, lie in the region [8,9]:

$$5 \times 10^{-11}\mathrm{eV}^2 \lesssim \Delta m^2 \lesssim 5 \times 10^{-10}\ \mathrm{eV}^2, \tag{1}$$

$$0.6 \lesssim \sin^2 2\theta \leq 1.0. \tag{2}$$

Although this result is obtained utilizing the standard solar model predictions of ref. [16] for the fluxes of the *pp*, *pep*, ^{7}Be, ^{8}B and CNO neutrinos, it is rather stable with respect to variation of the fluxes within their estimated uncertainty ranges [7,9]. If, for instance, one treats the total ^{8}B neutrino flux as a free parameter in the mean event rate data analysis, the solution regions located within the limits determined by eqs. (1) and (2) change somewhat their position and magnitude only. In this case two new "low ^{8}B neutrino flux" solution regions appear [7] (at 95% C.L.) at $\sin^2 2\theta \gtrsim 0.6$ for $\Delta m^2 \sim (3-4) \times 10^{-11}$ eV^2 and $\Delta m^2 \sim (4-8) \times 10^{-12}$ eV^2 (for a recent analysis see [9]). For values of $\Delta m^2 \sim (4-8) \times 10^{-12}$ eV^2 the effects of the vacuum $\nu_e \leftrightarrow \nu_{\mu(\tau)}$ oscillations on the flux of ^{8}B neutrinos with energies $E_\nu \gtrsim 5$ MeV, which is presently studied in the Super-Kamiokande experiment and will be studied in the near future with the SNO detector, are hardly observable. This low ^{8}B flux vacuum oscillation (VO) solution can be tested [7] in the future solar neutrino experiments BOREXINO, HELLAZ, etc., and we will not discuss it further.

When the current Super-Kamiokande results on the recoil-e^- spectrum [8] are added in the analysis of the solar neutrino data, the regions of values of Δm^2 and $\sin^2 2\theta$ for which the vacuum oscillations provide a good quality fit of the data, are considerably reduced and the best fit is achieved for $\Delta m^2 \cong (4.3-4.4) \times 10^{-10}$ eV^2 and $\sin^2 2\theta \cong 0.9$. Actually, the present Super-Kamiokande data on the spectrum of the recoil electrons from the solar (^{8}B) neutrino induced reaction $\nu + e^- \to \nu + e^-$ favors the $\nu_e \leftrightarrow \nu_{\mu(\tau)}$ vacuum oscillation solution of the solar neutrino problem over the MSW solutions [8].

A strong evidence (if not a proof) that the solar neutrinos take part in vacuum oscillations on the way to the Earth would be the observation of a seasonal variation effect which differs from the standard geometrical one (see the second and the third articles quoted in [1] as well as [4–7,17–21]). For values of Δm^2 from the VO solution region (1) and neutrino energies $\mathrm{E}_\nu \gtrsim 5$ MeV, the oscillation length in vacuum, $\mathrm{L_v} = 4\pi \mathrm{E}_\nu / \Delta \mathrm{m}^2$, is of the order of, or exceeds but not by a very large factor, the seasonal change of the distance between the Sun and the Earth, $\Delta \mathrm{R} = 2\epsilon \mathrm{R}_0$, where $\epsilon = 0.0167$ is the ellipticity of the Earth orbit around the Sun and $\mathrm{R}_0 = 1.496 \times 10^8$ km is the mean Sun-Earth distance. This leads to a noticeable dependence of the neutrino oscillation probability on the Sun-Earth distance, which in turn can create a specific seasonal difference in the solar neutrino signals in detectors like Super-Kamiokande, SNO and ICARUS. This difference should be particularly large in the signals due to the

[1] The possibility of solar $\nu_e \leftrightarrow \nu_s$ oscillations, ν_s being a sterile neutrino, is disfavored by the existing solar neutrino data [5,7,9].

0.862 MeV ^{7}Be neutrinos [6], to be studied with the BOREXINO detector. No analogous effect is predicted in the case of the MSW solution of the solar neutrino problem [22].

The seasonal effect due to the vacuum oscillations of solar neutrinos can be amplified or reduced by the standard geometrical one caused by the 6.68% decrease of the solar neutrino flux at the Earth surface when the Earth moves from perihelion (taking place in January) to aphelion (reached in July) on its orbit around the Sun [6]. In general, the VO induced seasonal effect in the solar neutrino signals in the Super-Kamiokande, SNO and ICARUS detectors is predicted to be relatively small for values of Δm^2 from the interval (1). For the envisaged and already attained rather low threshold e^--kinetic energy of detection of the recoil electrons in the Super-Kamiokande experiment $T_{e,Th} \cong 5$ MeV [8], the relative seasonal change of the event rate caused by the vacuum oscillations alone cannot exceed (even under the most favorable experimental conditions) approximately 10% [6] (see further). This is below the sensitivity currently reached in the search for this effect in the Super-Kamiokande experiment. For the $\nu_e \leftrightarrow \nu_{\mu(\tau)}$ oscillations of interest the effect in the Super-Kamiokande detector is reduced, in particular, by the weak neutral current interaction contribution of the $\nu_{\mu(\tau)}$ to the solar neutrino induced event rate. Correspondingly, the VO induced seasonal variation of the solar neutrino signal should be, in principle, somewhat larger (by a factor $\sim$ 1.2) in the charged current event rates in the SNO and ICARUS experiments. Nevertheless, the increase is not dramatic and it is worthwhile considering possible strategies which might lead to the enhancement of the seasonal effect in the samples of solar neutrino events collected by these or other real time detectors studying the ^{8}B neutrino flux.

It was noticed in ref. [6] that the magnitude of the seasonal effect generated by the vacuum solar ν_e oscillations in the Super-Kamiokande solar neutrino signal, and more generally in the solar neutrino signals in detectors based on the reaction $\nu + e^- \to \nu + e^-$, is very sensitive to the change of the threshold e^--kinetic energy from $T_{e,Th} \cong 5$ MeV to $T_{e,Th} \cong 7$ MeV. The VO induced seasonal effect in the signals in the SNO and ICARUS detectors should exhibit similar strong dependence on the chosen minimal value of the energy of the detected final state e^-. In the present article we explore this observation. We study in detail the threshold energy dependence of the seasonal variation effect in the sample of solar neutrino events in the Super-Kamiokande detector in the case of the vacuum oscillation solution of the solar neutrino problem. We show, in particular, that for the values of Δm^2 and $\sin^2 2\theta$ from the VO solution region (1) - (2), the predicted time and threshold e^- kinetic energy ($T_{e,Th}$) dependence of the energy integrated solar neutrino induced event rate factorize. The VO generated seasonal variation asymmetry is given by a product of a function which depends on $T_{e,Th}$ but does not depend on time, and of the standard geometrical asymmetry. We show also that for any given Δm^2 and $\sin^2 2\theta$ from the VO solution region there exists at least one value of the threshold energy $T_{e,Th}$ from the interval $(5 - 11)$ MeV, for which the seasonal variation effect in the solar neutrino sample of events, formed by recoil electrons with energy $T_e \geq T_{e,Th}$, is either maximal or very close to maximal. This suggests a possible strategy to search effectively for the VO induced seasonal effect: it consists in forming a set of samples of solar neutrino events, corresponding to a sufficiently large number of different values of $T_{e,Th}$ from the above interval, say, to $T_{e,Th} = 5;\ 6;\ 7; ...;\ 11$ MeV, and by measuring the seasonal variation in each of these samples. Predictions for the magnitude of the seasonal effect in each of the indicated samples for a large set of representative values of Δm^2 and $\sin^2 2\theta$ from the VO solution region are also given.

2. The Seasonal Variation Effect Observables

We shall consider the simplest case of solar $\nu_e \leftrightarrow \nu_{\mu(\tau)}$ oscillations generated by two-neutrino mixing. The probability that a solar electron neutrino with energy E_ν will not change into $\nu_{\mu(\tau)}$ on its way to the Earth when $\nu_e \leftrightarrow \nu_{\mu(\tau)}$ oscillations take place, has the well-known form:

$$\mathrm{P}(\nu_\mathrm{e} \to \nu_\mathrm{e}; \mathrm{R(t)}, \mathrm{E}_\nu) \equiv \mathrm{P(R(t))} \equiv \mathrm{P(t)} = 1 - \frac{1}{2}\sin^2 2\theta\ [1 - \cos 2\pi \frac{\mathrm{R(t)}}{\mathrm{L_v}}], \tag{3}$$

where $\mathrm{L_v} = 4\pi \mathrm{E}_\nu/\Delta m^2$ is the oscillation length in vacuum,

$$\mathrm{R(t)} = \mathrm{R}_0\ [1 - \epsilon \cos 2\pi \frac{\mathrm{t}}{\mathrm{T}}] \equiv \mathrm{R}_0\ \hat{\mathrm{R}}(\mathrm{t}), \tag{4}$$

is the Sun–Earth distance at time t of the year, $\mathrm{T} = 365.24$ days, $\mathrm{R}_0 = 1.496 \times 10^8$ km, $\hat{\mathrm{R}}(\mathrm{t})$ and $\epsilon = 0.0167$ being the mean Sun–Earth distance, the Sun-Earth distance at time t in A.U. and the ellipticity of the Earth orbit around the Sun.

It is not difficult to check that in the neutrino energy interval of interest, $\mathrm{E}_\nu \cong (5.0 - 14.4)$ MeV, the probability P(t) has, as a function of E_ν, i) one minimum for values of $\Delta m^2 \cong (0.5 - 0.8) \times 10^{-10}$ eV^2, ii) one maximum and one minimum for $\Delta m^2 \cong (0.8 - 2.0) \times 10^{-10}$ eV^2, etc.; for $\Delta m^2 \cong (4.3 - 4.4) \times 10^{-10}$ eV^2 it has 4 maxima and 3 minima. If, for instance, $\Delta m^2 = 0.75 \times 10^{-10}$ eV^2, P(t) decreases monotonically for E_ν rising in the interval $\mathrm{E}_\nu = (5.0 - 9.05)$ MeV, and increases with E_ν for $\mathrm{E}_\nu = (9.05 - 14.4)$ MeV; for $\Delta m^2 = 2.0 \times 10^{-10}$ eV^2 it decreases as E_ν increases in the two intervals $\mathrm{E}_\nu = (5.0 - 8.04)$ MeV and $\mathrm{E}_\nu = (12.06 - 14.4)$ MeV, and increases with E_ν in the interval $\mathrm{E}_\nu = (8.04 - 12.06)$ MeV. As it is easy to see from eq. (3), the derivatives of P(t) with respect to E_ν and R(t) have opposite signs [18]. Correspondingly, P(t) will decrease from January to June in the neutrino energy intervals, in which P(t) increases with E_ν, and it will increase from January to June in the energy intervals where P(t) decreases with E_ν, the seasonal effect having opposite signs in the two cases. There is no seasonal change of P(t) in the points of the extrema. Since the magnitude of the seasonal variation effect due to the vacuum oscillations is determined by the seasonal change of the oscillation probability P(t), it should be clear from the above discussion that for the VO solution values of Δm^2 from (1), the seasonal effect in the solar neutrino induced event rate integrated over the entire energy interval $\mathrm{E}_\nu = (5.0 - 14.4)$ MeV can be reduced considerably as a result of the mutual compensation between the opposite sign seasonal effects in the E_ν subintervals where P(t) increases and decreases with E_ν. As we shall see, for certain values of Δm^2 the compensation in the signal of the Super-Kamiokande detector is practically complete. We shall demonstrate in what follows that the indicated partial or complete compensation can be avoided in at least one of the samples of events corresponding to different minimal values of the recoil-e$^-$ kinetic energy, i.e., threshold energies $\mathrm{T_{e,Th}}$, from the interval $\mathrm{T_e} \cong (5 - 11)$ MeV.

The solar neutrino induced event rate in the Super-Kamiokande detector at time t of the year can be written for fixed threshold energy $\mathrm{T_{e,Th}}$, Δm^2 and $\sin^2 2\theta$ in the form:

$$\mathrm{R(t, T_{e,Th}}; \Delta m^2, \theta) \equiv \mathrm{R(t, T_{e,Th})} = \ < \ \frac{1}{\hat{\mathrm{R}}^2(\mathrm{t})}\ [\mathrm{r}_\nu + (1 - \mathrm{r}_\nu)\mathrm{P(t)}] \ > \ , \tag{5a}$$

where by the "average" of a quantity X, $< X >$, we shall understand in what follows

$$< X > \; = \frac{\mathrm{F(B)}}{\mathrm{R_0^2}} \int\limits_{\mathrm{T_{e,Th}}} \mathrm{dT_e} \int\limits_{\mathrm{T_e(1+\frac{m_e}{2T_e})}} \mathrm{dE_\nu \; X \; n(E_\nu) \; (d\sigma(\nu_e e^-)/dT_e)}. \qquad (5b)$$

Here $\mathrm{F(B)/R_0^2} \equiv \bar{\Phi}(\mathrm{B})$ is the mean annual ^{8}B neutrino flux at the Earth surface, $\mathrm{n(E_\nu)}$ is the normalized spectrum of ^{8}B neutrinos, $\int\limits_0^{14.4\ \mathrm{MeV}} \mathrm{n(E_\nu)dE_\nu} = 1$, $\mathrm{d\sigma(\nu_l e^-)/dT_e}$ is the differential cross–section of the process $\nu_l + e^- \rightarrow \nu_l + e^-$, $l = e, \mu \; (\tau)$, and $\mathrm{r_\nu = (d\sigma(\nu_\mu e^-)/dT_e)/(d\sigma(\nu_e e^-)/dT_e)}$. In the neutrino energy interval of interest one has $\mathrm{r_\nu} \cong (0.155 - 0.160)$. Expression (5b) is valid for ideal $\mathrm{e^-}$ detection efficiency and energy resolution of the Super-Kamiokande detector [2]. It can be trivially modified to include the latter. The time-dependent quantities in the expression for $\mathrm{R(t, T_{e,Th})}$ are the Sun-Earth distance, i.e., the geometrical factor (expressed in A.U.), $\hat{\mathrm{R}}^{-2}\mathrm{(t)}$, and the probability P(t).

In what follows we shall consider the event rate $\mathrm{R(t; T_{e,Th})}$, averaged over a time interval with a central point $\mathrm{t = t_c}$ and width Δt, $\mathrm{R(t_c, \Delta t; T_{e,Th})}$. The point $\mathrm{t_c}$ can be the time at which the Earth reaches the perihelion, $\mathrm{t_c = t_p = 0}$, or aphelion, $\mathrm{t_c = t_a = T/2}$, or any other chosen time of the year. It is convenient to choose $\mathrm{t_p = 0 \leq t_c \leq t_a = T/2}$ since $\mathrm{R(t_c) = R(T - t_c)}$. The seasonal effect due to VO should exhibit a similar symmetry. We shall present results for $\mathrm{t_c = t_p;\ t_p + T/12;\ t_p + 2T/12; ...;\ t_a}$ and a width of one month, $\Delta\mathrm{t = T/12}$. In their analysis of the solar neutrino data the Super-Kamiokande collaboration is utilizing time bins having a width of 1.5 months, $\Delta\mathrm{t = T/8}$ [8]. As we shall see, the choice of $\Delta\mathrm{t} \gtrsim \mathrm{T/4}$ tends to suppress the seasonal variation effect.

Obviously, the time-averaged event rate $\mathrm{R(t_c, \Delta t; T_{e,Th})}$ is determined by the time-averaged probability P(t). It proves useful to consider two different types of time-averaging. The first includes the effect of the geometrical factor,

$$\bar{\mathrm{P}}_{\mathrm{GF}}(\mathrm{t_c}, \Delta\mathrm{t}) = \frac{1}{\Delta\mathrm{t}} \int\limits_{\mathrm{t_c - \frac{1}{2}\Delta t}}^{\mathrm{t_c + \frac{1}{2}\Delta t}} \mathrm{dt} \; \frac{\mathrm{P(t)}}{\hat{\mathrm{R}}^2\mathrm{(t)}} \; , \qquad (6)$$

while in the second the geometrical factor effect is essentially eliminated:

$$\bar{\mathrm{P}}_{\mathrm{NGF}}(\mathrm{t_c}, \Delta\mathrm{t}) = \frac{\bar{\mathrm{P}}_{\mathrm{GF}}(\mathrm{t_c}, \Delta\mathrm{t})}{\kappa(\mathrm{t_c}, \Delta\mathrm{t})} \; , \qquad (7)$$

where

$$\kappa(\mathrm{t_c}, \Delta\mathrm{t}) = \frac{1}{\Delta\mathrm{t}} \int\limits_{\mathrm{t_c - \frac{1}{2}\Delta t}}^{\mathrm{t_c + \frac{1}{2}\Delta t}\ dt} \frac{\mathrm{dt}}{\hat{\mathrm{R}}^2\mathrm{(t)}} \; = 1 + 2\epsilon \cos\left(2\pi \frac{\mathrm{t_c}}{\mathrm{T}}\right) \; \frac{\sin 2\pi\Delta\mathrm{t/(2T)}}{2\pi\Delta\mathrm{t/(2T)}} + O(\epsilon^2), \qquad (8)$$

---

[2]Obviously, expressions (5a) and (5b) and the results based on them we shall obtain, are valid for any other "ideal" detector utilizing the $\nu + e^- \rightarrow \nu + e^-$ reaction for detection of the ^{8}B neutrinos. In this sense our results can serve as a guidance for the expected $\mathrm{T_{e,Th}}-$dependence of the magnitude of the seasonal effect in any detector of this type.

and we have used eq. (4) and the fact that terms $\sim \epsilon^2 \cong 2.8 \times 10^{-4}$ are beyond the sensitivity of the operating and planned solar neutrino experiments and can be neglected. It follows from eqs. (4) and (6) - (8) that the one year averaged probabilities $\bar{\rm P}_{\rm GF}({\rm t_c}, {\rm T})$ and $\bar{\rm P}_{\rm NGF}({\rm t_c}, {\rm T})$ practically coincide:

$$\bar{\rm P}_{\rm GF}({\rm t_c}, {\rm T}) = \bar{\rm P}_{\rm NGF}({\rm t_c}, {\rm T}) + O(\epsilon^2). \tag{9}$$

The same result holds for the average probabilities independently of $\Delta{\rm t}$ for ${\rm t_c} = {\rm T}/4;\ 3{\rm T}/4$, i.e., at the spring and autumn equinoxes: $\bar{\rm P}_{\rm GF}({\rm t_c} = {\rm T}/4\ (3{\rm T}/4), \Delta{\rm t}) = \bar{\rm P}_{\rm NGF}({\rm t_c} = {\rm T}/4\ (3{\rm T}/4), \Delta{\rm t}) + O(\epsilon^2)$.

The expression for the average event rate in the time interval $[{\rm t_c} - \Delta{\rm t}/2, {\rm t_c} + \Delta{\rm t}/2]$, in which the effect of the geometrical factor is essentially excluded, ${\rm R}_{\rm NGF}({\rm t_c}, \Delta{\rm t}; {\rm T_{e,Th}})$, can formally be obtained from eqs. (5a) - (5b) by replacing the probability ${\rm P(t)}$ with the probability $\bar{\rm P}_{\rm NGF}({\rm t_c}, \Delta{\rm t})$ and by setting the factor $\hat{\rm R}^{-2}({\rm t})$ to 1:

$$ {\rm R}_{\rm NGF}({\rm t_c}, \Delta{\rm t}; {\rm T_{e,Th}}) = \ < \ {\rm r}_\nu + (1 - {\rm r}_\nu)\bar{\rm P}_{\rm NGF}({\rm t_c}, \Delta{\rm t}) \ > \ . \tag{10}$$

It is easy to see from eqs. (5) - (8) and (10) and the above remark that for the average event rate containing the contribution of the geometrical factor, ${\rm R}_{\rm GF}({\rm t_c}, \Delta{\rm t}; {\rm T_{e,Th}})$, one has:

$$ {\rm R}_{\rm GF}({\rm t_c}, \Delta{\rm t}; {\rm T_{e,Th}}) = \kappa({\rm t_c}, \Delta{\rm t})\ {\rm R}_{\rm NGF}({\rm t_c}, \Delta{\rm t}; {\rm T_{e,Th}}). \tag{11}$$

The one year averaged event rates ${\rm R}_{\rm GF}({\rm t_c}, {\rm T}; {\rm T_{e,Th}})$ and ${\rm R}_{\rm NGF}({\rm t_c}, {\rm T}; {\rm T_{e,Th}})$ coincide up to corrections $\sim \epsilon^2$. For $\rm t_c$ corresponding to the perihelion, ${\rm t_c} = 0$, we shall denote them both by [3] ${\rm R}({\rm T_{e,Th}})$: ${\rm R}({\rm T_{e,Th}}) \equiv {\rm R}_{\rm NGF}(0, {\rm T}; {\rm T_{e,Th}}) \cong {\rm R}_{\rm GF}(0, {\rm T}; {\rm T_{e,Th}})$.

We shall analyze in what follows two observables: the ratio

$$ {\rm N_i}({\rm t_c}, \Delta{\rm t}; {\rm T_{e,Th}}) = \frac{{\rm R_i}({\rm t_c}, \Delta{\rm t}; {\rm T_{e,Th}})}{{\rm R}({\rm T_{e,Th}})}\ ,\ {\rm i} = {\rm NGF},\ {\rm GF}, \tag{12}$$

and the related seasonal variation asymmetry,

$$ {\rm A_i^{seas}}({\rm t_c}, \Delta{\rm t}; {\rm T_{e,Th}}) = {\rm N_i}({\rm t_c}, \Delta{\rm t}; {\rm T_{e,Th}}) - {\rm N_i}({\rm t_c} + {\rm T}/2, \Delta{\rm t}; {\rm T_{e,Th}})\ ,\ {\rm i} = {\rm NGF},\ {\rm GF}. \tag{13}$$

Since ${\rm N_i}({\rm t_c} + {\rm T}/2, \Delta{\rm t}; {\rm T_{e,Th}}) = {\rm N_i}({\rm T}/2 - {\rm t_c}, \Delta{\rm t}; {\rm T_{e,Th}})$, it is sufficient to consider $0 \leq {\rm t_c} \leq {\rm T}/4$ in the case of the asymmetry. Note that both observables (12) and (13) do not depend on the total flux of ^{8}B neutrinos. The observable ${\rm N}_{\rm NGF}({\rm t_c}, \Delta{\rm t}; {\rm T_{e,Th}})$ coincides with the one introduced in ref. [6]. The seasonal variation asymmetries which have been analyzed in refs. [17–21] are analogous to, but differ somewhat from, ${\rm A}^{\rm seas}_{\rm NGF(GF)}({\rm t_c}, \Delta{\rm t}; {\rm T_{e,Th}})$.

In the absence of neutrino oscillations ${\rm P(t)} = 1$ and we have: ${\rm N}_{\rm NGF}({\rm t_c}, \Delta{\rm t}; {\rm T_{e,Th}}) = 1$, ${\rm N}_{\rm GF}({\rm t_c}, \Delta{\rm t}; {\rm T_{e,Th}}) = \kappa({\rm t_c}, \Delta{\rm t})$, ${\rm A}^{\rm seas}_{\rm NGF}({\rm t_c}, \Delta{\rm t}; {\rm T_{e,Th}}) = 0$, and ${\rm A}^{\rm seas}_{\rm GF}({\rm t_c}, \Delta{\rm t}; {\rm T_{e,Th}}) = {\rm A}^{\rm seas}_{\rm geom}({\rm t_c}, \Delta{\rm t})$, where ${\rm A}^{\rm seas}_{\rm geom}({\rm t_c}, \Delta{\rm t})$ is the seasonal asymmetry of purely geometrical origin,

$$ {\rm A}^{\rm seas}_{\rm geom}({\rm t_c}, \Delta{\rm t}) = \kappa({\rm t_c}, \Delta{\rm t}) - \kappa({\rm t_c} + {\rm T}/2, \Delta{\rm t}) = 4\epsilon \cos\left(2\pi\frac{\rm t_c}{\rm T}\right)\ \frac{\sin 2\pi\Delta{\rm t}/(2{\rm T})}{2\pi\Delta{\rm t}/(2{\rm T})} + {\rm O}(\epsilon^2). \tag{14}$$

---

[3] Note, that the perihelion was reached on 2, 5, and 4 of January in 1997, 1998 and 1999, respectively.

For $0 \leq t_c < T/4$ (and $\Delta t < T$) the geometrical asymmetry is positive: $A^{seas}_{geom}(t_c, \Delta t) > 0$.

As can be shown, the following simple relations hold true up to corrections $\sim 10^{-3}$ if the solar ν_e take part in two-neutrino oscillations $\nu_e \leftrightarrow \nu_{\mu(\tau)}$ with $\Delta m^2 \lesssim 5 \times 10^{-10}$ eV^2:

$$N_{NGF}(t_c, \Delta t; T_{e,Th}) = 1 + \frac{1}{2}\, W(T_{e,Th})\; A^{seas}_{geom}(t_c, \Delta t) + O(10^{-3}), \tag{15}$$

$$\begin{aligned} N_{GF}(t_c, \Delta t; T_{e,Th}) &= N_{NGF}(t_c, \Delta t; T_{e,Th}) + \frac{1}{2} A^{seas}_{geom}(t_c, \Delta t) + O(10^{-3}) \\ &= 1 + \frac{1}{2}\; (1 + W(T_{e,Th}))\; A^{seas}_{geom}(t_c, \Delta t) + O(10^{-3}), \end{aligned} \tag{16}$$

$$A^{seas}_{NGF}(t_c, \Delta t; T_{e,Th}) = W(T_{e,Th})\; A^{seas}_{geom}(t_c, \Delta t) + O(10^{-3}), \tag{17}$$

$$\begin{aligned} A^{seas}_{GF}(t_c, \Delta t; T_{e,Th}) &= A^{seas}_{NGF}(t_c, \Delta t; T_{e,Th}) + A^{seas}_{geom}(t_c, \Delta t) + O(10^{-3}) \\ &= (1 + W(T_{e,Th}))\; A^{seas}_{geom}(t_c, \Delta t) + O(10^{-3}). \end{aligned} \tag{18}$$

The factor $W(T_{e,Th})$ in eqs. (15) - (18) does not depend on the time variables t_c and Δt and is given by:

$$W(T_{e,Th}) = \frac{1}{2} \sin^2 2\theta\; \frac{< \; (1 - r_\nu) \pi \frac{R_0}{L_v}\; \sin 2\pi \frac{R_0}{L_v} \; >}{< \; r_\nu + (1 - r_\nu) P(R_0) \; >}\;, \tag{19}$$

where $P(R_0)$ is the one year average probability, i.e., $P(R(t))$, eq. (3), in which the Sun-Earth distance $R(t)$ is replaced with the mean Sun-Earth distance R_0. In the case of absence of oscillations we have $\sin^2 2\theta = 0$ and/or $\Delta m^2 = 0$, and therefore $W(T_{e,Th}) = 0$.

The relations (15) - (18) can be derived using the following observations. For $\Delta m^2 \lesssim 5 \times 10^{-10}$eV^2 and $E_\nu \geq 5$ MeV we have $2\pi\epsilon R_0/L_v \lesssim 0.63$. Correspondingly, one can expand the probability $P(R(t))$ in power series of $x(t) = 2\pi\epsilon R_0/L_v \cos 2\pi t/T$ [6]. In this way one obtains:

$$P(R(t)) = P(R_0) + \Delta P(t), \tag{20}$$

where

$$\Delta P(t) = \frac{1}{2} \sin^2 2\theta \left[(x(t) - \frac{1}{6} x^3(t) + ...) \sin 2\pi \frac{R_0}{L_v} - \frac{1}{2} (x^2(t) - \frac{1}{12} x^4(t) + ...) \cos 2\pi \frac{R_0}{L_v} \right]. \tag{21}$$

For $\Delta m^2 \leq 10^{-10}$ eV^2 and $E_\nu \geq 5$ MeV one finds $x(t) \leq 0.13$. Thus, the term linear in $x(t)$ gives the dominant contribution in $\Delta P(t)$: for the contribution of the quadratic term, for instance, we get $0.25 x^2(t) \leq 4.3 \times 10^{-3}$. Keeping only the term linear in $x(t)$ in the expression for $\Delta P(t)$ one arrives at the relations (15) - (19). The linear approximation, as numerical studies we have performed showed, turns out to be equally accurate for 10^{-10}eV$^2 < \Delta m^2 \leq 5 \times 10^{-10}$ eV^2. The reason for this somewhat unexpected result lies in the fact that for $\Delta m^2 \geq 10^{-10}$ eV^2 and $E_\nu \sim (5 - 14)$ MeV, the argument of the $t-$independent sine and cosine functions in $\Delta P(t)$ is relatively large: $2\pi R_0/L_v \geq (2.7 - 7.5)$. Thus, for $\Delta m^2 \geq 10^{-10}$ eV^2, the functions $(2\pi\epsilon R_0/L_v)^n \sin 2\pi R_0/L_v$ and $(2\pi\epsilon R_0/L_v)^n \cos 2\pi R_0/L_v$ with $n \geq 2$ are fastly oscillating functions of E_ν and the integration over the neutrino energy renders them negligible:

$$< \frac{1}{2(n!)} (2\pi\epsilon R_0/L_v)^n \sin(2\pi R_0/L_v) > \quad \sim O(10^{-3}), \quad n \geq 3, \tag{22a}$$

$$< \frac{1}{2(\mathrm{n}!)}(2\pi\epsilon \mathrm{R}_0/\mathrm{L}_\mathrm{v})^\mathrm{n}\cos(2\pi \mathrm{R}_0/\mathrm{L}_\mathrm{v}) > \quad \sim \mathrm{O}(10^{-3}), \quad \mathrm{n} \geq 2. \tag{22b}$$

Relations (17) and (18) imply that to a high degree of accuracy the VO generated seasonal variation asymmetries $\mathrm{A}^{\mathrm{seas}}_{\mathrm{NGF,GF}}(\mathrm{t_c}, \Delta\mathrm{t}; \mathrm{T_{e,Th}})$ are proportional to the geometrical one, $\mathrm{A}^{\mathrm{seas}}_{\mathrm{NGF(GF)}}(\mathrm{t_c}, \Delta\mathrm{t}; \mathrm{T_{e,Th}}) \sim \mathrm{A}^{\mathrm{seas}}_{\mathrm{geom}}(\mathrm{t_c}, \Delta\mathrm{t})$. Actually, the time ($t_c$ and Δt) and the energy dependencies of the observables $\mathrm{N_{NGF,GF}}(\mathrm{t_c}, \Delta\mathrm{t}; \mathrm{T_{e,Th}})$ and $\mathrm{A}^{\mathrm{seas}}_{\mathrm{NGF,GF}}(\mathrm{t_c}, \Delta\mathrm{t}; \mathrm{T_{e,Th}})$ factorize: the whole time dependence is contained in $\mathrm{A}^{\mathrm{seas}}_{\mathrm{geom}}(\mathrm{t_c}, \Delta\mathrm{t})$ and is given with a high precision by the factor

$$\mathrm{f}(\mathrm{t_c}, \Delta\mathrm{t}) = \cos\left(2\pi\frac{\mathrm{t_c}}{\mathrm{T}}\right) \ \frac{\sin 2\pi\Delta\mathrm{t}/(2\mathrm{T})}{2\pi\Delta\mathrm{t}/(2\mathrm{T})}, \tag{23}$$

while the function $\mathrm{W}(\mathrm{T_{e,Th}})$ carries all the information about the energy dependence. Depending on the values of Δm^2 from the interval (1) and on $\mathrm{T_{e,Th}}$, the function $\mathrm{W}(\mathrm{T_{e,Th}})$ can be positive, negative or zero for $\mathrm{E}_\nu \cong (5.0 - 14.4)$ MeV; and $|\mathrm{W}(\mathrm{T_{e,Th}})|$ can be greater or smaller than 1 (see Table III). Correspondingly, the VO generated and the geometrical seasonal asymmetries $\mathrm{A}^{\mathrm{seas}}_{\mathrm{NGF}}$ and $\mathrm{A}^{\mathrm{seas}}_{\mathrm{geom}}$ can have the same or opposite signs and the former can be larger or smaller in absolute value than the latter [6]. The asymmetry which contains both the VO induced seasonal effect and the effect due to the geometrical factor, $\mathrm{A}^{\mathrm{seas}}_{\mathrm{GF}}$, is just equal to the sum of the seasonal asymmetry due to the VO only and of the geometrical asymmetry, eq. (18). The asymmetry $\mathrm{A}^{\mathrm{seas}}_{\mathrm{GF}}$ can be close to zero due to mutual cancelation between $\mathrm{A}^{\mathrm{seas}}_{\mathrm{NGF}}$ and $\mathrm{A}^{\mathrm{seas}}_{\mathrm{geom}}$ [6]. This implies, in particular, that one cannot have simultaneously $|\mathrm{A}^{\mathrm{seas}}_{\mathrm{NGF}}| \ll \mathrm{A}^{\mathrm{seas}}_{\mathrm{geom}}$ and $|\mathrm{A}^{\mathrm{seas}}_{\mathrm{GF}}| \ll \mathrm{A}^{\mathrm{seas}}_{\mathrm{geom}}$ for the same set of values of the parameters. However, one of the two asymmetries, $\mathrm{A}^{\mathrm{seas}}_{\mathrm{NGF}}$ or $\mathrm{A}^{\mathrm{seas}}_{\mathrm{GF}}$, can be strongly suppressed, while the other can have observable values. All these possibilities are realized for the values of Δm^2, $\sin^2 2\theta$, E_ν and $\mathrm{T_{e,Th}}$ of interest (see further and Figs. 1 and 2).

Let us note that in ref. [17] a Fourier analysis of the predicted time dependence of the event rate in, e.g., the Super-Kamiokande detector in the case of the VO solution of the solar neutrino problem was performed. The coefficients in the corresponding Fourier expansion were found to be expressed in terms of Bessel functions. The authors of ref. [17] noticed that the constant and the first harmonic term dominate in the expansion. The origin of this result becomes clear from eqs. (15) - (18) and (22a) - (22b).

We expect eqs. (15) - (18) and the above conclusions to be valid for the charged current solar neutrino event rates and the corresponding seasonal variation asymmetries to be measured with, e.g., the SNO and ICARUS detectors. The expressions for the observables (12) and (13) and for the function (19) for the SNO detector can be obtained simply by modifying the definition of the "average" in eqs. (5b) and of the averaged quantities in eqs. (10) and (19): one has to set $\mathrm{r}_\nu = 0$ and replace in (5b) $\mathrm{d}\sigma(\nu_\mathrm{e}\mathrm{e}^-)/\mathrm{dT_e}$ with $\mathrm{d}\sigma(\nu_\mathrm{e}\mathrm{d} \to \mathrm{e}^-\mathrm{pp})/\mathrm{dT_e}$ - the differential cross-section of the charged current reaction $\nu_e + \mathrm{d} \to e^- + \mathrm{p} + \mathrm{p}$, changing as well the lower limit of integration over E_ν to $\mathrm{T_e} + 1.44$ MeV. It should also be emphasized that our general results (15) - (19) will not change if one includes in the analysis the e^-−detection efficiency and energy resolution of a specific detector as long as they do not vary with time.

Let us note that in the case of averaging over a time period not exceeding two months, $\Delta\mathrm{t} \leq \mathrm{T}/6$, we have

$$\kappa(t_c, \Delta t) = 1 + 2\epsilon\cos\left(2\pi\frac{t_c}{T}\right) + O(\sim 1.7 \times 10^{-3}), \tag{24}$$

$$A^{seas}_{geom}(t_c, \Delta t) = 4\epsilon \cos\left(2\pi \frac{t_c}{T}\right) + O(\sim 3.4 \times 10^{-3}), \quad (25)$$

and both quantities are practically $\Delta t-$independent. The geometrical asymmetry is maximal if t_c is chosen to be the time when the Earth is at perihelion: $A^{seas}_{geom}(t_c = 0, \Delta t \leq T/6) \cong 4\epsilon = 6.68\%$. As it follows from eqs. (14) - (18), averaging over a time interval exceeding 3 months, $\Delta t \gtrsim T/4$, suppresses the seasonal variation effect.

3. Enhancing the Seasonal Variation Effect

We have performed numerical calculations of the observables (12) and (13) for a large representative set of values of the parameters Δm^2 and $\sin^2 2\theta$ from the VO solution region (1) - (2), which are given in Table I. Some of our results are presented in Tables I - III and in Figs. 1 - 3. The threshold energy dependence of the event rate ratio (12), $N_{NGF}(t_c, \Delta t; T_{e,Th})$, is shown for six selected values of Δm^2 and $\sin^2 2\theta$ from the set and for $t_c = 0$ (perihelion); T/12; 2T/12; ...; $t_a = T/2$ (aphelion) and $\Delta t = T/12$ in Fig. 1. The perihelion-aphelion asymmetries $A^{seas}_{NGF,GF}(t_p = 0, \Delta t = T/12; T_{e,Th}) \equiv A^{seas}_{NGF,GF}(T_{e,Th})$ (see eq. (13)) are plotted as functions of $T_{e,Th}$ in Fig. 2 for all the values of Δm^2 and $\sin^2 2\theta$ given in the first column of Table I. As Figs. 1 and 2 demonstrate, depending on Δm^2 and $\sin^2 2\theta$, for $T_{e,Th} \cong 5$ MeV the seasonal effect due to VO can be maximal or close to the maximal (Figs. 1a and 2a, $\Delta m^2 = 0.5 \times 10^{-10}$ eV^2, $\sin^2 2\theta = 0.9$), or can be strongly suppressed (Figs. 1b, 1e, 1f and 2a, 2c, $\Delta m^2 = 0.7$; 2.5; 4.4 $\times 10^{-10}$ eV^2). With the increase of $T_{e,Th}$ from the value of $\sim$ 5 MeV, the VO induced seasonal effect can change drastically. For $\Delta m^2 = 0.9 \times 10^{-10}$ eV^2 and $\sin^2 2\theta = 1.0$ (Figs. 1c and 2b), for instance, it is negative and close to maximal in absolute value at $T_{e,Th} \cong 5$ MeV, goes through zero at $T_{e,Th} \cong 8.5$ MeV and is positive for larger values of $T_{e,Th}$ reaching a maximum at $T_{e,Th} \cong 12$ MeV. If, however, $\Delta m^2 = 0.4 \times 10^{-10}$ eV^2, it decreases monotonically with the increase of $T_{e,Th}$ (Fig. 2a), while for $\Delta m^2 = 1.3 \times 10^{-10}$ eV^2 the effect is negative and hardly observable at $T_{e,Th} \cong 5$ MeV, but increases in absolute value reaching a maximum at $T_{e,Th} \cong 10.9$ MeV, $A^{seas}_{NGF}(T_{e,Th} \cong 10.9 \text{ MeV}) \cong -14.1\%$ (Figs. 1d and 2c).

In the case of relatively large values of $\Delta m^2 \cong (2.0 - 4.4) \times 10^{-10}$ eV^2 the seasonal effect due to VO is relatively small or negligible for 5 MeV $\leq T_{e,Th} \lesssim 7.5$ MeV (Figs. 1e, 1f and 2c). For $\Delta m^2 \cong 4.4 \times 10^{-10}$ eV^2 and $\sin^2 2\theta \cong 0.9$ the VO induced seasonal asymmetry increases with $T_{e,Th}$ reaching a maximum at $T_{e,Th} \cong 10.1$ MeV, $A^{seas}_{NGF}(T_{e,Th} = 10.1 \text{ MeV}) \cong 14.8\%$, then decreases to zero at $T_{e,Th} \cong 12.2$ MeV and becomes negative for larger values of $T_{e,Th}$. The geometrical effect amplifies the asymmetry in the region of the maximum and $A^{seas}_{GF}(T_{e,Th} = 10.1 \text{ MeV}) \cong 21.5\%$ (Fig. 2c). At $T_{e,Th} \cong 9.5$ (11.0) MeV, we have for the indicated values of Δm^2 and $\sin^2 2\theta$: $A^{seas}_{NGF} \cong 13.0$ (10.0)%. Including the realistic experimental conditions in the calculations of the asymmetry will reduce its magnitude, but not considerably - by $\sim (1 \div 2)\%$. The change of $T_{e,Th}$ from 5 MeV to 10.1 MeV will increase the statistical error of the measured value of $A^{seas}_{GF}(T_{e,Th})$ (see Table I). Nevertheless, values of $A^{seas}_{NGF(GF)}(T_{e,Th}) \sim 15$ (21)%, as the one obtained above for $\Delta m^2 \cong 4.4 \times 10^{-10}$ eV^2 at $T_{e,Th} \cong 10.1$ MeV, can already be tested with the Super-Kamiokande detector [8].

In Table II we give the numerical values of $A^{seas}_{NGF}(T_{e,Th})$ at $T_{e,Th} = 5$; 6; 7; 8; 9; 10; 11 MeV for the chosen representative set of values of Δm^2 and $\sin^2 2\theta$ from the VO solution region. For each pair of the latter, the values of $A^{seas}_{NGF}(T_{e,Th})$ corresponding to a maximum

of $|A^{seas}_{NGF}(T_{e,Th})|$ in the interval $T_{e,Th} = (5 - 11)$ MeV, $A^{seas,max}_{NGF}$, and the $T_{e,Th}$ at which the maximum is reached, $T^{max}_{e,Th}$, are also given. For the set of values of neutrino parameters we have considered, the minimal $A^{seas,max}_{NGF}$ is 2.2%; for most of the values, however, $|A^{seas,max}_{NGF}| \gtrsim 4.5\%$, with the maximal values of the asymmetry reaching $\sim (10 \div 15)\%$. Our results show, in particular, that for any given Δm^2 from the VO solution region (1) there exists at least one value of $T_{e,Th}$ from the interval $(5 - 11)$ MeV, for which the seasonal variation effect in the solar neutrino sample of events with recoil electrons having $T_e \geq T_{e,Th}$ is either *maximal* or *very close to maximal* (in absolute value). Since the precise value of Δm^2 is still unknown, this implies that one can effectively search for the seasonal effect by forming a set of samples of solar neutrino events, which correspond to a sufficiently large number of different values of $T_{e,Th}$ from the above interval, say, for those in Tables I - III, and by measuring the seasonal variation in each of these samples. As we have already emphasized, the seasonal effect can change dramatically with the sample.

The correlation between the magnitude of the seasonal asymmetry and the electron threshold kinetic energy $T_{e,Th}$ discussed above is a manifestation of the fact that the underlying statistical distribution of neutrino events in the case of interest is a bivariate function of time and energy, whose marginal distributions are the one-year average electron spectrum and the energy integrated time dependence. An example of a possible graphical representation of such a bivariate distribution of the (ν, e^-) events is given in Fig. 3a. The figure corresponds to $\Delta m^2 = 0.7 \times 10^{-10}$ eV^2 and $\sin^2 2\theta = 0.85$. Each color represents a specific value of the one month average event rate ratio $N_{NGF}(t_c, \Delta t = T/12; T_{e,Th})$, eq. (12), calculated for $t_c = 0$ (perihelion); $T/12$; $2T/12$; ...; $t_a = T/2$ (aphelion). Other types of representations are possible, of course, but the tests we have performed indicate that this one is better suited for optimizing the efficiency of the information extraction. These maps allow to compare at a glance the predicted time and energy dependence of the ratio $N_{NGF}(t_c, \Delta t; T_{e,Th})$ for different values of Δm^2 and $\sin^2 2\theta$. For example, Fig. 3a clearly shows that for the chosen Δm^2 and $\sin^2 2\theta$ no observable time modulation is expected at $T_{e,Th} \cong 5$ MeV, while the maximal modulation takes place for $T_{e,Th} \cong 9.5$ MeV. When applied to real data, the presentation technique used to generate Fig. 3a will produce an "image" of the bivariate event rate distribution, similar to usual astronomical images obtained by X-rays or γ-rays telescopes. If the solar neutrino problem is indeed caused by vacuum oscillations of solar neutrinos, the event rate distribution "images" will be characterized by a pattern composed of elongated *spots* of different intensity, whose distribution and shape are functions of the neutrino parameters Δm^2 and $\sin^2 2\theta$. It should be possible to analyze such images using well tested techniques, as those commonly applied for imaging in high energy astronomy in order to ensure not only the presence of relevant patterns, but also their consistency with the vacuum oscillations scenario, discarding in this way subtle systematical errors induced, for instance, by background time variability.

As we have shown, for the ^{8}B neutrino induced event rates of interest and the VO solution neutrino parameters from the region (1) - (2) one has:

$$N_{NGF}(t_c, \Delta t; T_{e,Th}) = q(T_{e,Th}) + m(T_{e,Th}, \Delta t)\ \cos 2\pi \frac{t_c}{T} + O(10^{-3})\ , \qquad (26)$$

where q is a function of $T_{e,Th}$, m depends both on $T_{e,Th}$ and on the sampling interval Δt, but both q and m do not depend on t_c. If the data does not exhibit any time dependence, apart from that caused by the geometrical effect which is removed from $N_{NGF}(t_c, \Delta t; T_{e,Th})$, one

should have $m(T_{e,Th}, \Delta t) = 0$. The signature of vacuum oscillations is a significant threshold energy dependent deviation of $m(T_{e,Th}, \Delta t)$ from zero. For the choice [6] of the event rate normalization, eq. (12), we have $q(T_{e,Th}) = 1$ for any sampling scheme (see eq. (15)) and, as it follows from eqs. (14), (15) and (26),

$$m(T_{e,Th}, \Delta t) = 2\epsilon W(T_{e,Th}) \, \frac{\sin 2\pi \Delta t/(2T)}{2\pi \Delta t/(2T)} \, , \tag{27}$$

where $W(T_{e,Th})$ is given in eq. (19). These relations do not necessarily hold true for event rate normalizations which differ from that used by us. Equation (26) allows to reduce the bivariate distribution $N_{NGF}(t_c, \Delta t; T_{e,Th})$ to the univariate distribution $m(T_{e,Th}, \Delta t)$ without information loss, to the extent that eq. (26) represents a good approximation to the true time dependence. In Fig. 3b we compare the time dependence of the one month average event rates $N_{NGF}(t_c, \Delta t = T/12; T_{e,Th})$ computed utilizing eqs. (5a), (5b) and (12) (points with crosses), with those obtained using eq. (26), for $T_{e,Th} = 5.0$ MeV (solid line), 7.5 MeV (dotted line) and 10.0 MeV (dash-dotted line). As Fig. 3b indicates, eq. (26) describes the time-dependence of $N_{NGF}(t_c, \Delta t = T/12; T_{e,Th})$ with a very high accuracy. This is confirmed by a detailed analysis based on the standard Pearson index, performed for Δm^2 in the range $(0.1 \div 4.4) \times 10^{-10}$ eV^2, $\sin^2 2\theta \leq 1$ and $T_{e,Th} < 14.0$ MeV. The accuracy of eq. (26) increases quickly with the increasing of the magnitude of the seasonal asymmetry. The largest errors occur for combinations of Δm^2, $\sin^2 2\theta$ and $T_{e,Th}$ for which the predicted NGF asymmetry is negligible, i.e., is smaller than 0.6%. It is not surprising that eq. (26) is very accurate even for Δm^2 as large as 4.4×10^{-10} eV^2 given the results obtained at the end of the previous Section (see eqs. (20) - (22) and the related discussion).

As we have already indicated, the function $W(T_{e,Th})$ carries all the information about the threshold energy dependence of the event rates and the seasonal asymmetries of interest, eqs. (15) - (18); its knowledge allows to reconstruct the time dependence of the normalized event rates (12). Figure 3c and Table III illustrate the dependence of W on $T_{e,Th}$ for the representative set of values of the neutrino parameters Δm^2 and $\sin^2 2\theta$. The function $W(T_{e,Th})$ was calculated numerically by fitting the time-dependence of $N_{NGF}(t_c, T/12; T_{e,Th})$ (computed without any approximations) with that of eq. (26), utilizing the least squares method. The maximal value of $W(T_{e,Th})$ for each pair of Δm^2 and $\sin^2 2\theta$, W^{max}, and the value of $T_{e,Th}$ at which it takes place, $T^{max}_{e,Th}$, are also given in Table III.

Let us consider an alternative event rate normalization and the corresponding version of eq. (26), i.e., $R_{NGF}(t_c, \Delta t; T_{e,Th})/R_{SSM}(T_{e,Th}) = q'(T_{e,Th}) + m'(T_{e,Th}, \Delta t) \cos 2\pi t_c/T$, where $q'(T_{e,Th}) \neq 1$ represents the "distortion" of the one year average event rate distribution and $R_{SSM}(T_{e,Th})$ is the one year average event rate predicted in a standard solar model in the absence of neutrino oscillations. Now $m'(T_{e,Th}, \Delta t)$ carries information about the amplitude of the time variation, while both $m'(T_{e,Th}, \Delta t)$ and $q'(T_{e,Th})$ determine the energy dependence. However, since they are related to the index $m(T_{e,Th}, \Delta t)$ in eq. (26) by $m(T_{e,Th}, \Delta t) = m'(T_{e,Th}, \Delta t)/q'(T_{e,Th}, \Delta t)$, it seems more convenient to use the normalization in eq. (12) leading to eq. (26) with only one function of $T_{e,Th}$ ($q(T_{e,Th}) = 1$), rather than having the $T_{e,Th}$ dependence spread in two functions.

If the geometrical effect is included in the event rate data, it can be accounted for in the observables (12) and (13), as it follows from eqs. (16) and (18), by simply adding 1 to the function $W(T_{e,Th})$ (e.g., in eq. (27)). This is a consequence of the normalization [6] used by us in eq. (12). There exist also simple

relations between the function $W(T_{e,Th})$ and the different types of seasonal asymmetries considered by other authors. For instance, relation (17) holds for the asymmetry $A'_{NGF}(\Delta t; T_{e,Th}) = 2(R_{NGF}(0, \Delta t; T_{e,Th}) - R_{NGF}(T/2, \Delta t; T_{e,Th})/(R_{NGF}(0, \Delta t; T_{e,Th}) + R_{NGF}(T/2, \Delta t; T_{e,Th})$. The asymmetry defined in [18] corresponds to $A_S = 2(R_{GF}(t_c = 0) - R_{GF}(t_c = T/2)/(R_{GF}(t_c = T/4) + R_{GF}(t_c = 3T/4))$ with $\Delta t = T/4$ and $T_{e,Th} = 6.5$ MeV and is given by $A_S = 4\epsilon\frac{2\sqrt{2}}{\pi}(1 + W(6.5 \text{ MeV}))$. Evidently, eq. (26) can be used to relate different seasonal asymmetries and spectral distortion functions discussed in the literature, while plots and tables like Fig. 3c and Table III can be utilized to make predictions for the latter for a large range of sampling schemes, $T_{e,Th}$ and values of the neutrino oscillation parameters.

4. Conclusions

We have studied in detail the threshold energy ($T_{e,Th}$) dependence of the seasonal variation effect in the electron energy integrated solar neutrino signal of the Super-Kamiokande detector in the case of the vacuum oscillation solution of the solar neutrino problem. We have shown that for the values of the neutrino oscillation parameters Δm^2 and $\sin^2 2\theta$ from the VO solution region (1) - (2), the time and the $T_{e,Th}$ dependence of the corresponding solar neutrino event rate factorize to a high degree of accuracy. This facorization takes a particularly simple form, eqs. (15) - (18), when the event rate for a given threshold energy $T_{e,Th}$ is normalized to the one year average event rate for the same threshold energy [6], eq. (12). As a consequence of the factorization, the VO induced seasonal variation asymmetry is proportional to the geometrical one, the coefficient of proportionality being a function of $T_{e,Th}$, but not of time. The asymmetry which contains both the VO induced and the geometrical seasonal effects, A^{seas}_{GF}, is just equal to the sum of the seasonal asymmetry due to the VO only, A^{seas}_{NGF}, and of the geometrical asymmetry A^{seas}_{geom} (eq. (18)). The asymmetries A^{seas}_{NGF} and A^{seas}_{geom} can mutually cancel and A^{seas}_{GF} can be close to zero [6]. This implies, in particular, that one cannot have simultaneously $|A^{seas}_{NGF}| \ll A^{seas}_{geom}$ and $|A^{seas}_{GF}| \ll A^{seas}_{geom}$ for the same set of values of the parameters. However, one of the two asymmetries, A^{seas}_{NGF} or A^{seas}_{GF}, can be strongly suppressed, while the other can have observable values. All these possibilities are realized for the values of Δm^2, $\sin^2 2\theta$, E_ν and $T_{e,Th}$ of interest.

The seasonal variation effect exhibits a strong dependence on $T_{e,Th}$. For the values $\Delta m^2 \cong (4.3 - 4.4) \times 10^{-10}$ eV^2 and $\sin^2 2\theta \cong 0.9$, suggested by the current Super-Kamiokande data on the e^-−spectrum [8], for instance, the VO induced seasonal asymmetry is negligible for $T_{e,Th} \cong (5 - 8)$ MeV, increases with $T_{e,Th}$ reaching a maximum at $T_{e,Th} \cong 10.1$ MeV, $A^{seas}_{NGF}(T_{e,Th} = 10.1 \text{ MeV}) \cong 14.8\%$, then decreases to zero at $T_{e,Th} \cong 12.2$ MeV and becomes negative for larger values of $T_{e,Th}$. The geometrical effect amplifies the asymmetry in the region of the maximum and $A^{seas}_{GF}(T_{e,Th} = 10.1 \text{ MeV}) \cong 21.5\%$ (Fig. 2c). At $T_{e,Th} \cong 9.5$ (11.0) MeV, we have for the indicated values of Δm^2 and $\sin^2 2\theta$: $A^{seas}_{NGF} \cong 13.0$ (10.0)% [4]. Results for other VO solution values of Δm^2 and $\sin^2 2\theta$ can be found in Table II.

[4] The quoted asymmetry values correspond to ideal experimental conditions; they will be somewhat smaller, by $\sim (1 - 2)\%$, if one takes into account the e^- detection efficiency and energy resolution of the Super-Kamiokande detector

We have shown also that for any given Δm^2 and $\sin^2 2\theta$ from the VO solution region (1) - (2) there exists at least one value of $T_{e,Th}$ from the interval $(5 - 11)$ MeV, for which the VO induced seasonal effect in the solar neutrino sample of events with recoil electrons having $T_e \geq T_{e,Th}$ is either *maximal* or *very close to maximal*. Given the fact that the precise values of Δm^2 and $\sin^2 2\theta$ are still unknown, this suggests that one can effectively search for the seasonal effect by forming a set of samples of solar neutrino events, which correspond to a sufficiently large number of different values of $T_{e,Th}$ from the above interval, say, for those in Tables I - III, $T_{e,Th} = 5$; 6; 7;...; 11 MeV, and by measuring the seasonal variation in each of these samples. The seasonal effect can change dramatically with the sample. The results summarized above are illustrated in Figs. 1 - 3 and Tables II - III. Although they have been derived for the Super-Kamiokande detector, we expect similar results to be valid for the SNO and ICARUS detectors.

Acknowledgements.

The work of S.T.P. was supported in part by the Italian MURST under the program "Fisica Teorica delle Interazioni Fondamentali" and by Grant PH-510 from the Bulgarian Science Foundation.

REFERENCES

[1] B. Pontecorvo, Zh. Eksp. Teor. Fiz. 53 (1967) 1717; V. Gibov and B. Pontecorvo, Phys. Lett. B28 (1969) 493; S.M. Bilenky and B. Pontecorvo, Phys. Rep. 41 (1978) 225.

[2] B. Pontecorvo, Zh. Eksp. Teor. Fiz. 33 (1957) 549; ibid. 34 (1958) 247; Z. Maki, M. Nakagawa and S. Sakata, Prog. Theor. Phys. 28 (1962) 870.

[3] S.M. Bilenky and S.T. Petcov, Rev. Mod. Phys. **59** (1987) 671.

[4] P.I. Krastev and S.T. Petcov, Phys. Lett. 285B (1992) 85; ibid. 299B (1993) 99; V. Barger et al., Phys. Rev. Lett. 69 (1992) 3135, and Phys. Rev. D43 (1991) 1110; A. Acker, S. Pakvasa and J. Pantaleone, Phys. Rev. Lett. 65 (1990) 2479, and Phys. Rev. D43 (1991) 1754; see also: S.L. Glashow and L.M. Krauss, Phys. Lett. 190B (1987) 199.

[5] P.I. Krastev and S.T. Petcov, Phys. Rev. Lett. 72 (1994) 1960.

[6] P.I. Krastev and S.T. Petcov, Nucl. Phys. B449 (1996) 605.

[7] P.I. Krastev and S.T. Petcov, Phys. Rev. D53 (1996) 1665.

[8] M. Smy, Super-Kamiokande Coll., Talk given at the DPF Conference, American Institute of Physics, January 5 - 7, 1999, Los Angeles (see the WWW page of the Conference: www.physics.ucla.edu/dpf99/trans/DPF99_Transparencies.htm).

[9] J.N. Bahcall, P.I. Krastev and A.Yu. Smirnov, Phys. Rev. D58 (1998) 096016.

[10] R. Davis et al., Prog. Part. Nucl. Phys. 32 (1994) 13; K. Lande, Homestake Coll., Talk given at the *Neutrino '98* International Conference [23], 1998.

[11] K.S. Hirata et al., Kamiokande Coll., Phys. Rev. Lett. 77 (1996) 1683.

[12] W. Hampel et al., GALLEX Coll., Phys. Lett. B388 (1996) 384; T. Kirsten, GALLEX Coll., Talk given at the *Neutrino '98* International Conference [23], 1998.

[13] D.N. Abdurashitov et al., SAGE Coll., Phys. Rev. Lett. 77 (1996) 4708; V. Gavrin, SAGE Coll., Talk given at the *Neutrino '98* International Conference [23], 1998.

[14] Y. Suzuki, Super-Kamiokande Coll., Talk given at the *Neutrino '98* International Conference [23], 1998; Y. Fukuda et al., Phys. Rev. Lett. 81 (1998) 1158.

[15] J.N. Bahcall, *Neutrino Astrophysics*, Cambridge University Press, Cambridge, 1989.

[16] J.N. Bahcall, S. Basu and M. Pinsonneault, Phys. Lett. B433 (1998) 1.

[17] B. Faid et al., Phys. Rev. D56 (1997) 4374; hep-ph/9805293.

[18] S.P. Mikheyev and A.Yu. Smirnov, Phys. Lett. B429 (1998) 343.

[19] S.L. Glashow, P.J. Kernan and L. Krauss, hep-ph/9808470.

[20] V. Berezinsky, G. Fiorentini and M. Lissia, hep-ph/9811352.

[21] V. Barger and K. Whisnant, hep-ph/9812273.

[22] S.T. Petcov and J. Rich, Phys. Lett. B224 (1989) 401.

[23] International Conference on Neutrino Physics and Astrophysics *Neutrino '98*, June 3 - 9, 1998, Takayama, Japan; WWW page: http://www-sk.icrr.u-tokyo.ac.jp/nu98.

TABLES

TABLE I. The ratio $R(T_{e,Th})/R(5\ MeV)$ of the one year average event rates due to ^8B neutrinos in $\nu - e^-$ detectors (Super-Kamiokande, etc.) for several values of $T_{e,Th}$ and for a set of values of Δm^2 and $\sin^2 2\theta$ from the VO solution region.

n		Δm^2 (10^{-10} eV^2)	$\sin^2 2\theta$	$T_{e,Th}$ (MeV) 5.5	6.0	7.0	8.0	9.0	10.0	11.0
no oscillations				0.84	0.69	0.44	0.26	0.14	0.06	0.02
1	——	0.40	1.00	0.86	0.73	0.50	0.31	0.17	0.08	0.03
2	·····	0.50	0.60	0.85	0.71	0.47	0.29	0.16	0.07	0.03
3	– · – ·	0.50	0.90	0.86	0.73	0.50	0.32	0.18	0.09	0.03
4	– – –	0.55	1.00	0.87	0.74	0.52	0.34	0.20	0.10	0.04
5	□	0.60	0.70	0.84	0.70	0.47	0.29	0.16	0.08	0.03
6	◇	0.60	0.90	0.85	0.72	0.49	0.31	0.18	0.09	0.03
7	⋆	0.65	0.85	0.84	0.70	0.47	0.29	0.17	0.08	0.03
8	△	0.70	0.85	0.82	0.67	0.44	0.27	0.16	0.08	0.03
9	——	0.75	0.80	0.81	0.65	0.42	0.25	0.14	0.07	0.03
10	·····	0.80	0.65	0.81	0.65	0.41	0.24	0.13	0.06	0.02
11	– · – ·	0.80	0.70	0.81	0.65	0.41	0.24	0.13	0.06	0.02
12	– – –	0.80	0.85	0.79	0.63	0.38	0.23	0.12	0.06	0.02
13	□	0.85	0.75	0.80	0.63	0.38	0.22	0.12	0.05	0.02
14	◇	0.85	1.00	0.75	0.56	0.31	0.17	0.09	0.04	0.02
15	⋆	0.90	0.75	0.79	0.62	0.37	0.21	0.11	0.05	0.02
16	△	0.90	1.00	0.75	0.55	0.29	0.15	0.07	0.03	0.01
17	——	1.00	0.75	0.79	0.62	0.36	0.19	0.09	0.04	0.02
18	·····	1.00	1.00	0.76	0.56	0.29	0.13	0.06	0.02	0.01
19	– · – ·	1.10	1.00	0.78	0.60	0.31	0.14	0.06	0.02	0.01
20	– – –	1.20	1.00	0.81	0.63	0.35	0.17	0.07	0.03	0.01
21	□	1.30	1.00	0.83	0.67	0.39	0.20	0.09	0.03	0.01
22	◇	2.50	0.90	0.83	0.67	0.39	0.22	0.12	0.07	0.03
23	⋆	4.40	0.90	0.83	0.68	0.44	0.25	0.13	0.07	0.03

TABLE II. The perihelion - aphelion asymmetry $A^{seas}_{NGF}(t_c = 0, \Delta t = T/12; T_{e,Th}) \equiv A^{seas}_{NGF}(T_{e,Th})$ in % for different values of $T_{e,Th}$ and a set of values of Δm^2 and $\sin^2 2\theta$ from the VO solution region. Given also are the values of the asymmetry corresponding to a maximum of $|A^{seas}_{NGF}|$ in the interval $T_{e,Th} = (5 - 11)$ MeV, $A^{seas,max}_{NGF}$, and the $T_{e,Th}$ at which it is reached, $T^{max}_{e,Th}$. The asymmetry including the geometrical effect $A^{seas}_{GF}(0, T/12; T_{e,Th}) = A^{seas}_{NGF}(T_{e,Th}) + 4\epsilon$.

Δm^2		$T^{max}_{e,Th}$		$T_{e,Th}$ (MeV)						
(10^{-10} eV^2)	$\sin^2 2\theta$	(MeV)	$A^{seas,max}_{NGF}$	5.0	6.0	7.0	8.0	9.0	10.0	11.0
0.40	1.00	5.00	4.05	4.05	3.73	3.38	3.04	2.73	2.45	2.20
0.50	0.60	6.28	2.16	2.08	2.16	2.14	2.05	1.94	1.81	1.68
0.50	0.90	5.66	4.46	4.41	4.43	4.24	3.94	3.62	3.29	2.99
0.55	1.00	6.07	6.39	6.02	6.39	6.24	5.83	5.34	4.83	4.36
0.60	0.70	7.98	3.10	2.22	2.75	3.02	3.10	3.04	2.91	2.75
0.60	0.90	7.45	5.25	4.03	4.90	5.23	5.19	4.95	4.61	4.25
0.65	0.85	8.54	4.82	2.46	3.71	4.48	4.79	4.79	4.61	4.34
0.70	0.85	9.46	5.00	0.97	2.63	3.92	4.67	4.97	4.97	4.79
0.75	0.80	10.85	4.43	-0.68	0.86	2.33	3.43	4.08	4.38	4.42
0.80	0.65	11.00	2.82	-1.38	-0.47	0.56	1.46	2.14	2.58	2.82
0.80	0.70	11.00	3.28	-1.60	-0.55	0.66	1.72	2.51	3.01	3.28
0.80	0.85	11.00	5.19	-2.56	-0.91	1.11	2.92	4.18	4.90	5.19
0.85	0.75	11.00	3.54	-3.01	-2.06	-0.64	0.84	2.08	2.99	3.54
0.85	1.00	11.00	8.99	-6.73	-5.18	-1.78	2.46	6.00	8.15	8.99
0.90	0.75	5.00	-3.89	-3.89	-3.33	-2.11	-0.58	0.90	2.13	2.99
0.90	1.00	5.29	-8.22	-8.12	-7.85	-5.64	-1.70	2.74	6.31	8.35
1.00	0.75	5.86	-5.07	-4.75	-5.06	-4.61	-3.49	-1.99	-0.39	1.03
1.00	1.00	6.72	-10.56	-8.68	-10.17	-10.49	-9.13	-5.85	-1.22	3.29
1.10	1.00	8.25	-12.24	-7.61	-9.77	-11.45	-12.23	-11.66	-9.33	-5.36
1.20	1.00	9.46	-13.40	-5.88	-8.18	-10.39	-12.15	-13.21	-13.24	-11.83
1.30	1.00	10.85	-14.11	-3.98	-6.15	-8.53	-10.69	-12.45	-13.68	-14.09
2.50	0.90	9.79	14.31	0.10	-0.12	0.87	7.10	13.18	14.01	11.44
4.40	0.90	10.13	14.75	0.92	1.04	2.34	1.62	8.59	14.69	9.99

TABLE III. Values of the function $W(T_{e,Th})$ for various $T_{e,Th}$ and Δm^2 and $\sin^2 2\theta$.

Δm^2		$T^{max}_{e,Th}$		$T_{e,Th}$ (MeV)						
(10^{-10} eV^2)	$\sin^2 2\theta$	(MeV)	W^{max}	5.0	6.0	7.0	8.0	9.0	10.0	11.0
0.40	1.00	5.00	0.61	0.61	0.56	0.51	0.46	0.41	0.37	0.33
0.50	0.60	6.17	0.33	0.32	0.33	0.32	0.31	0.29	0.27	0.25
0.50	0.90	5.51	0.68	0.67	0.67	0.64	0.60	0.55	0.50	0.45
0.55	1.00	6.17	0.97	0.91	0.97	0.95	0.88	0.81	0.73	0.66
0.60	0.70	8.02	0.47	0.34	0.42	0.46	0.47	0.46	0.44	0.42
0.60	0.90	7.30	0.80	0.61	0.74	0.79	0.79	0.75	0.70	0.64
0.65	0.85	8.49	0.73	0.38	0.56	0.68	0.73	0.73	0.70	0.66
0.70	0.85	9.50	0.76	0.15	0.40	0.60	0.71	0.75	0.75	0.73
0.75	0.80	10.63	0.67	-0.10	0.13	0.36	0.52	0.62	0.67	0.67
0.80	0.65	11.00	0.43	-0.21	-0.07	0.09	0.22	0.33	0.39	0.43
0.80	0.70	11.00	0.50	-0.24	-0.08	0.10	0.26	0.38	0.46	0.50
0.80	0.85	11.00	0.79	-0.39	-0.13	0.17	0.45	0.64	0.75	0.79
0.85	0.75	11.00	0.54	-0.45	-0.31	-0.09	0.13	0.32	0.46	0.54
0.85	1.00	11.00	1.37	-1.02	-0.78	-0.26	0.38	0.92	1.25	1.37
0.90	0.75	5.02	-0.59	-0.59	-0.50	-0.32	-0.08	0.14	0.33	0.46
0.90	1.00	5.41	-1.24	-1.23	-1.19	-0.85	-0.24	0.43	0.97	1.28
1.00	0.75	5.94	-0.77	-0.72	-0.77	-0.70	-0.53	-0.30	-0.05	0.16
1.00	1.00	6.78	-1.60	-1.32	-1.54	-1.59	-1.38	-0.87	-0.17	0.52
1.10	1.00	8.17	-1.85	-1.15	-1.48	-1.73	-1.85	-1.76	-1.41	-0.79
1.20	1.00	9.50	-2.03	-0.90	-1.24	-1.58	-1.84	-2.00	-2.00	-1.78
1.30	1.00	10.83	-2.14	-0.61	-0.94	-1.30	-1.62	-1.89	-2.07	-2.13
2.50	0.90	9.68	2.19	0.02	-0.02	0.14	1.10	2.04	2.14	1.73
4.40	0.90	10.05	2.30	0.14	0.16	0.37	0.25	1.35	2.29	1.50

FIGURE CAPTIONS

Figure 1. The t_c and $T_{e,Th}$ dependence of the normalized one month average event rate $N_{NGF}(t_c, \Delta t = T/12; T_{e,Th})$, eq. (12), in $\nu - e^-$ detectors (Super-Kamiokande, etc.) for six representative values of Δm^2 and $\sin^2 2\theta$ from the VO solution region, given in Table 1 under the numbers: n = 3 (a), 8 (b), 16 (c), 21 (d), 22 (e), 23 (f). The solid, dotted, dash-dotted, dashed lines and the lines with squares, diamonds, stars in each of the sub-figures (a) - (f) correspond to seven equally spaced values of $t_c = 0$ (perihelion); T/12; T/6; T/4; T/3; 5T/12; T/2, respectively. The seasonal asymmetry is given by $A^{seas}_{NGF}(t_c, T/12; T_{e,Th})$ = $N_{NGF}(t_c, T/12; T_{e,Th})$ - $N_{NGF}(T/2 - t_c, T/12; T_{e,Th})$, $0 \leq t_c \leq T/4$, and is maximal for $t_c = 0$.

Figure 2. The dependence of the perihelion - aphelion asymmetry $A^{seas}_{NGF}(t_c = 0, \Delta t = T/12; T_{e,Th})$ (in %), eq. (13), on $T_{e,Th}$ for different values of Δm^2 and $\sin^2 2\theta$ from the VO solution region. The curves in the panels (a), (b) and (c) correspond to the values of Δm^2 and $\sin^2 2\theta$ in Table I numbered, respectively: 1 - 8, 9 - 16 and 17 - 23. Each curve of a given type (solid, dashed, dash-dotted, etc.) is obtained for the values of Δm^2 and $\sin^2 2\theta$ which are marked with the symbol of the curve (solid line, dashed line, dash-dotted line etc.) in the second column of Table 1. The asymmetry which includes the geometrical effect $A^{seas}_{GF}(0, T/12; T_{e,Th})$ = $A^{seas}_{NGF}(0, T/12; T_{e,Th}) + 4\epsilon$, $4\epsilon = 6.68\%$, is also shown.

Figure 3. a). Am "image" of the one month average event rate ratio (distribution) $N_{NGF}(t_c, T/12; T_{e,Th})$ (eq. (12)). Each vertical stripe corresponds to $t_c = 0$; T/12; T/6; T/4; ...; T, as is indicated on the horizontal axis. The vertical scale on the right-hand side allows to convert a color into a value of the ratio. b) The event rate ratio shown in a), plotted as a function of $\cos 2\pi t_c/T$ for $T_{e,Th} = 5.0$ MeV (solid line), 7.5 MeV (dotted line), 10.0 MeV (dashed-dotted line). The lines are the best fits to the computed ratio indicated by "+". c) The dependence of $W(T_{e,Th})$ on $T_{e,Th}$. All results shown in the figure are derived for $\Delta m^2 = 0.70 \times 10^{-10}$ eV^2 and $\sin^2 2\theta = 0.85$.

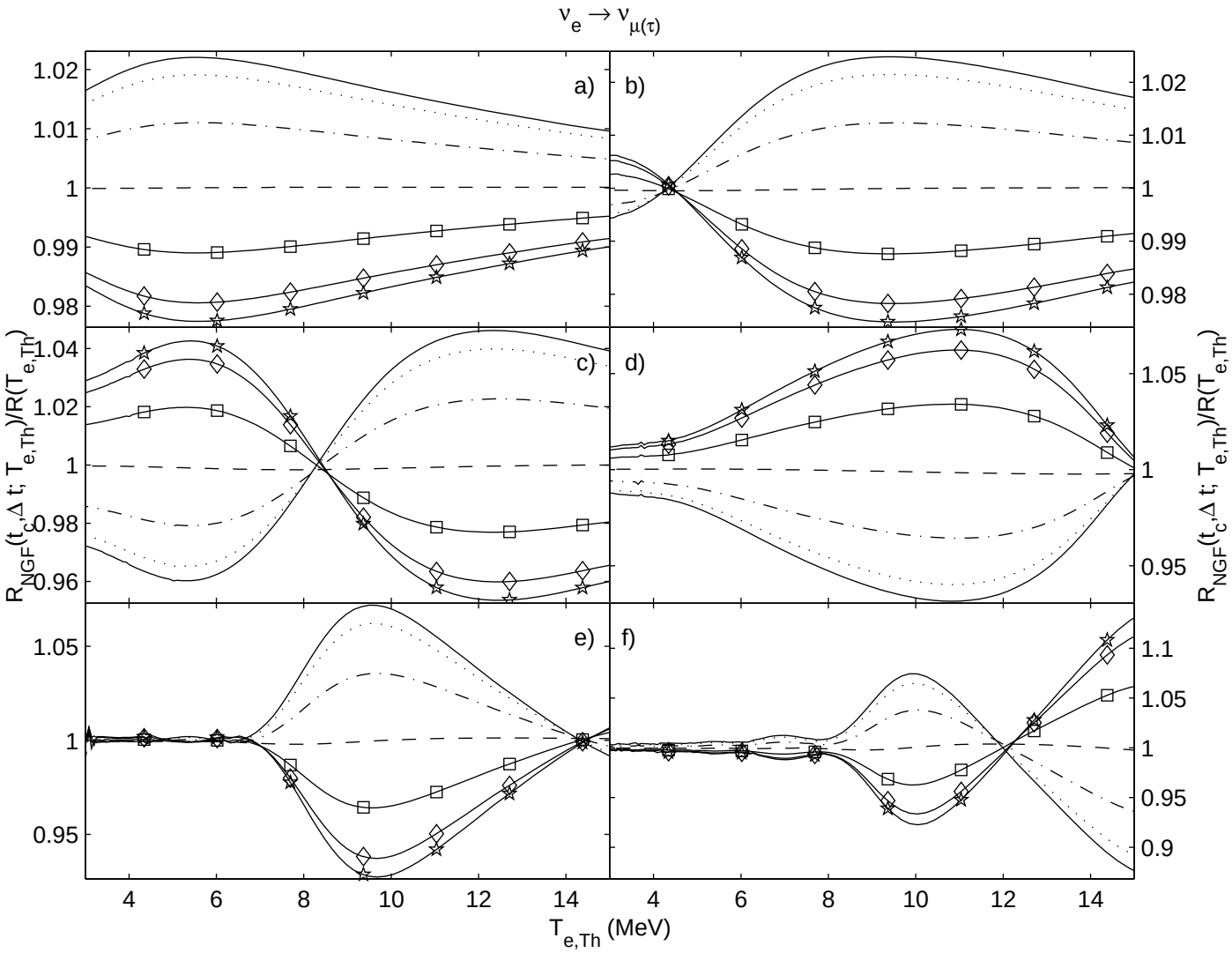
$\nu_e \rightarrow \nu_{\mu(\tau)}$
a)
b)
c)
d)
e)
f)
$R_{NGF}(t_c,\Delta t; T_{e,Th})/R(T_{e,Th})$
$T_{e,Th}$ (MeV)

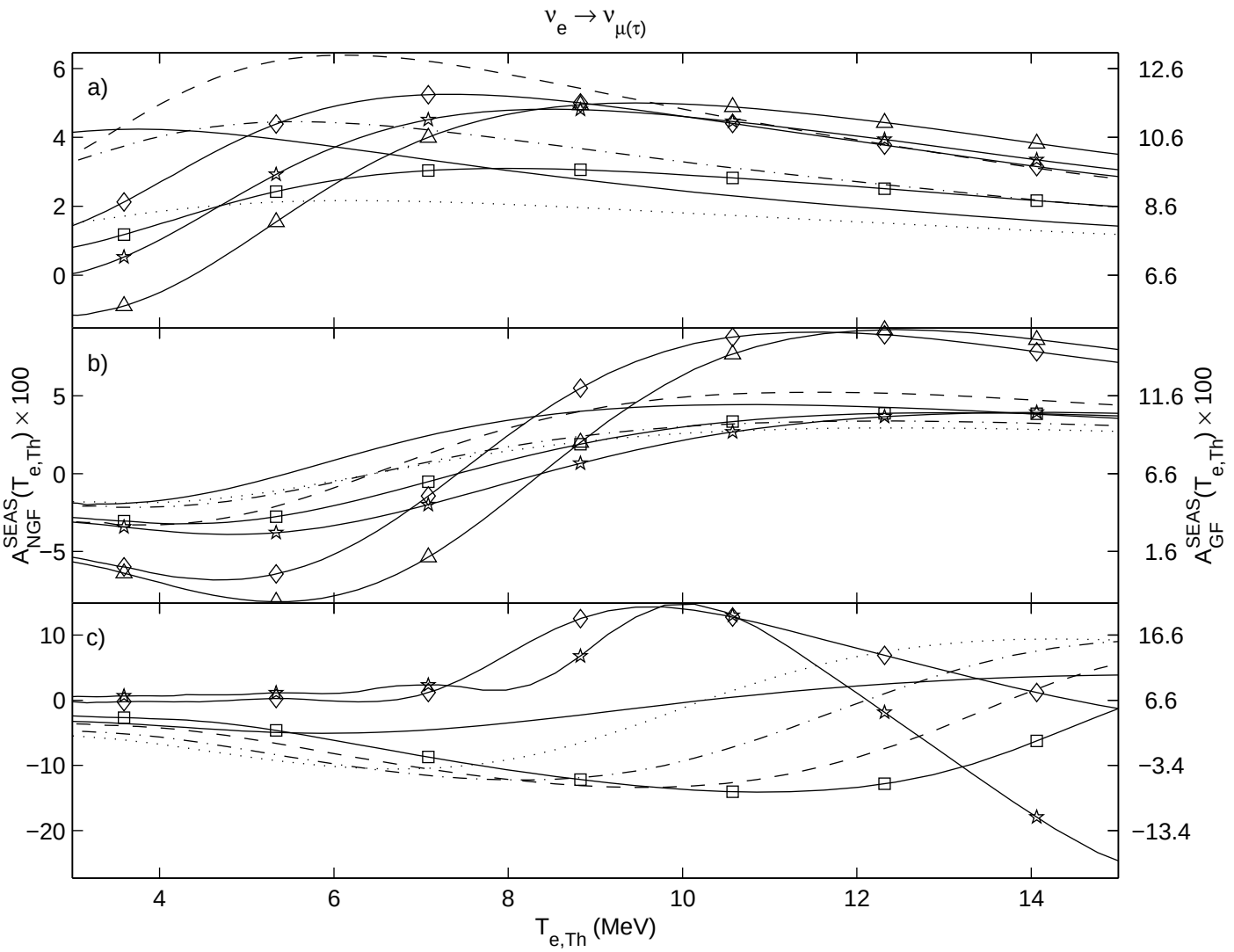
$\nu_e \rightarrow \nu_{\mu(\tau)}$
a)
b)
c)
$A^{SEAS}_{NGF}(T_{e,Th}) \times 100$
$A^{SEAS}_{GF}(T_{e,Th}) \times 100$
$T_{e,Th}$ (MeV)
6
4
2
0
12.6
10.6
8.6
6.6
5
−5
11.6
6.6
1.6
10
0
−10
−20
16.6
6.6
−3.4
−13.4
4
6
8
10
12
14

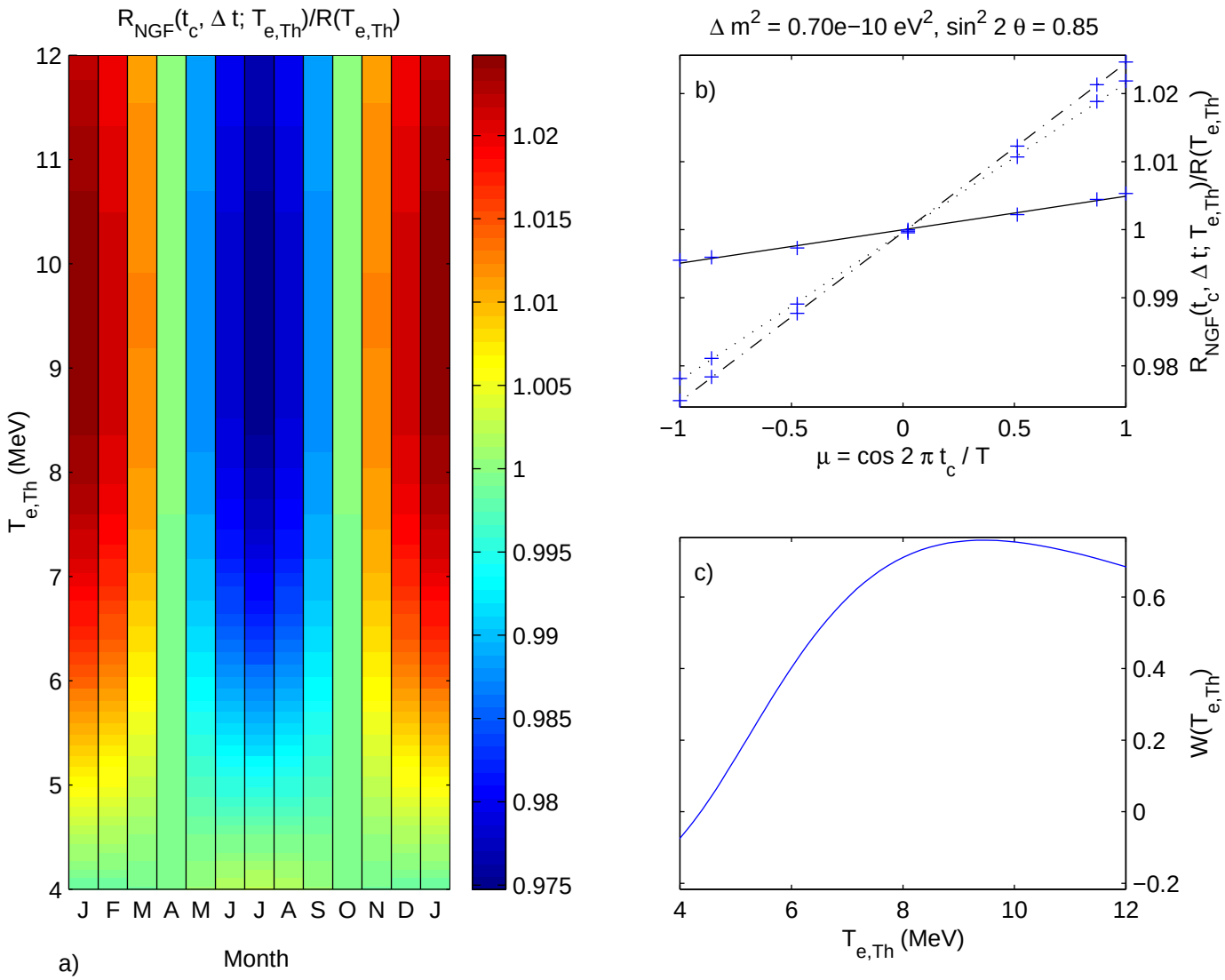
$R_{NGF}(t_c, \Delta t; T_{e,Th})/R(T_{e,Th})$
12
11
10
9
8
7
6
5
4
$T_{e,Th}$ (MeV)
J F M A M J J A S O N D J
Month
a)
1.02
1.015
1.01
1.005
1
0.995
0.99
0.985
0.98
0.975
$\Delta m^2 = 0.70e{-}10$ eV^2, $\sin^2 2\theta = 0.85$
b)
−1
−0.5
0
0.5
1
$\mu = \cos 2\pi t_c / T$
1.02
1.01
1
0.99
0.98
$R_{NGF}(t_c, \Delta t; T_{e,Th})/R(T_{e,Th})$
c)
4
6
8
10
12
$T_{e,Th}$ (MeV)
0.6
0.4
0.2
0
−0.2
$W(T_{e,Th})$